Editors' Suggestion

Quantum Degenerate Fermi Gas in an Orbital Optical Lattice

M. Hachmann,[1,2] Y. Kiefer,[1,2] J. Riebesehl,[1] R. Eichberger,[1,2] and A. Hemmerich[1,2,3]
[1]Institut für Laserphysik, Universität Hamburg, 22761 Hamburg, Germany
[2]Zentrum für Optische Quantentechnologien, Universität Hamburg, 22761 Hamburg, Germany
[3]The Hamburg Center for Ultrafast Imaging, Universität Hamburg, 22761 Hamburg, Germany

(Received 30 November 2020; accepted 21 June 2021; published 14 July 2021)

Spin-polarized samples and spin mixtures of quantum degenerate fermionic atoms are prepared in selected excited Bloch bands of an optical checkerboard square lattice. For the spin-polarized case, extreme band lifetimes above 10 s are observed, reflecting the suppression of collisions by Pauli's exclusion principle. For spin mixtures, lifetimes are reduced by an order of magnitude by two-body collisions between different spin components, but still remarkably large values of about 1 s are found. By analyzing momentum spectra, we can directly observe the orbital character of the optical lattice. The observations demonstrated here form the basis for exploring the physics of Fermi gases with two paired spin components in orbital optical lattices, including the regime of unitarity.

DOI: 10.1103/PhysRevLett.127.033201

Optical lattices are synthetic arrays of bosonic or fermionic neutral atoms or molecules trapped in laser-induced periodic potentials [1]. Aside from their practical use in atomic clock applications [2] they are celebrated as an ideal toolbox for quantum simulation of lattice physics [3–6]. Their usefulness in the context of quantum simulation of electronic crystalline matter requires in particular the use of fermionic particles, which assume the role of the electrons tunneling and interacting in a lattice of ionic cores. In fact, there is a promising strain of research devoted to emulate the fermionic Hubbard model [7] and to experimentally explore its phase diagram [8–14], which on the theory side even with modern computational power has remained an open challenge. However, many of the intriguing functionalities of crystalline electronic condensed matter rely on orbital degrees of freedom, which play a decisive role for metal-insulator transitions, superconductivity, and colossal magnetoresistance in transition-metal oxides [15,16]. Orbital p-like single-particle wave functions have been recently simulated with electrons in the second band of an artificial square lattice formed by an array of carbon monoxide molecules on a Cu(111) surface [17]. It is however not obvious how this scenario could be extended to emulate many-body physics. A natural but insufficient approach to extend optical lattices with fermionic atoms to include higher Bloch bands is to load sufficiently many atoms [18]. This, however, requires multiply occupied lattice sites and, hence, leads to deleterious collisions of more than two particles resulting in excessive loss and heating in connection with molecule formation [19,20].

An alternative approach, that was pioneered for bosonic atoms, selectively excites the atoms from the lowest band into a desired higher target band, thus keeping the site occupation low [21–24]. The underlying strategy is that the functionality of interest takes place in a higher band and does not discriminate between a filled or an empty lowest band. There is reason to assume that two-body collisions would lead to immediate band relaxation. However, theoretical [25,26] and experimental [21,24] research has shown that with appropriately designed lattice geometries reasonably long lifetimes can be realized, which has triggered widespread interest in optical lattices with orbital character [27].

For the first time, similar techniques are used in this work to form fermionic optical lattices with orbital degrees of freedom, which should prove useful as an advanced generation of quantum simulators for electronic matter beyond s-band lattice physics. For spin-polarized samples and mixtures of two spin components, the efficiency, with which selected excited bands can be occupied, as well as the corresponding lifetimes are shown to notably exceed the previous findings for bosons. We present exemplary results on the loading efficiency for the second, fourth, and seventh bands, but also higher bands can be addressed. For spin-polarized samples, we observe lifetimes above 10 s, limited by technical heating processes. Binary collisions, expected to be suppressed by Pauli's principle, are observed to play no role in this case. In contrast, for spin mixtures, two-body collisions between different spin components are observed to reduce the lifetimes. However, reasonably large values on the order of 1 s are also found in this case. Momentum spectroscopy confirms the orbital character of the formed wave functions. The techniques shown here form the basis for exploring the physics of Fermi gases with two paired spin components in orbital optical lattices, including the regime of unitarity, and hence may provide new fundamental insights into

 © 2021 American Physical Society

fermionic superfluidity in the presence of orbital degrees of freedom [28–37].

As the initial step in our experiments, a spin-polarized degenerate Fermi gas of up to 2.5×10^5 potassium atoms (^{40}K) in the hyperfine state $|F = 9/2, m_F = 9/2\rangle$ with a temperature $T = 0.18T_F$ is produced in an optical dipole trap, formed by two crossed laser beams with a wavelength of 1064 nm. Radio-frequency techniques can be optionally applied to prepare balanced spin mixtures of $|F = 9/2, m_F = -9/2\rangle$ (spin-up) and $|F = 9/2, m_F = -7/2\rangle$ (spin-down) atoms (see Ref. [38] for details). The atoms are adiabatically loaded into a bipartite optical square lattice, formed by two mutually orthogonal optical standing waves with the same wavelength $\lambda = 1064$ nm and aligned along the x and y axes, respectively. The optical standing waves are formed in a Michelson-Sagnac interferometer that provides precision control of the associated band structure (see Ref. [38] for details). The resulting lattice potential is composed of deep and shallow potential wells arranged as the black and white squares of a checkerboard, denoted $\mathcal{A}$ and $\mathcal{B}$, respectively [24]. In the xy plane, the lattice potential is approximated by

$$V(x, y) = -V_0[\cos^2(kx) + \cos^2(ky)] - \frac{1}{2}\Delta V \cos(kx)\cos(ky), \quad (1)$$

with the wave number $k = 2\pi/\lambda$. Along the z direction the atoms are weakly confined by an approximately harmonic potential, such that the lattice wells acquire a tubular shape. The potential depth $V_0 \geq 0$ and the potential difference between $\mathcal{A}$ wells and $\mathcal{B}$ wells, $\Delta V \in V_0 \times [-4, 4]$, can be controlled much faster than all relevant dynamical timescales. The lattice geometry in the xy plane is sketched in Fig. 1(a) for $\Delta V = 0$ and $\Delta V < 0$ in the left- and right-hand panels, respectively. In Fig. 1(b), sections through the lattice potential along the dashed lines in Fig. 1(a) are shown. For $\Delta V = 0$, a monopartite lattice (i.e., with equal $\mathcal{A}$ and $\mathcal{B}$ wells) is formed. Negative ΔV indicates deep $\mathcal{A}$ wells and shallow $\mathcal{B}$ wells and vice versa for positive ΔV.

After the atoms (spin-polarized or spin mixtures) are loaded to the lowest Bloch band of the optical lattice by slowly ramping up V_0 from zero to $5 - 15E_{\mathrm{rec}}$ in 150 ms, a quench protocol similar to that previously applied to bosonic atoms is used to transfer them into a selected higher Bloch band. Here, $E_{\mathrm{rec}} \equiv \hbar^2 k^2/2m$ denotes the single-photon recoil energy and m the atomic mass. The central step is to rapidly tune ΔV from negative to positive values in typically 100 μs. This technique has been summarized for bosons in Ref. [24] and a more detailed explanation adapted to the present work with fermions is provided in Ref. [38]. The populations of the Bloch bands are observed by means of a standard technique referred to as band mapping (cf. Ref. [38]).

In Fig. 2(a) band mapping images for spin-polarized samples are shown without excitation to higher bands [Fig. 2(a1)] and after the excitation protocol is applied to selectively excite the atoms to the second, fourth, and seventh

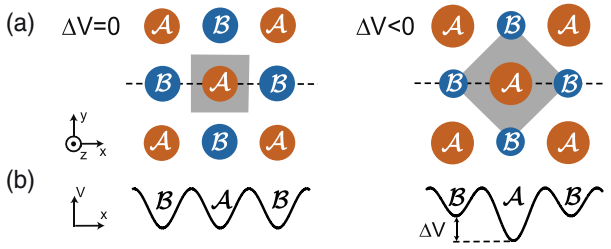

FIG. 1. (a) Lattice geometry in the xy plane for $\Delta V = 0$ (left) and $\Delta V < 0$ (right). The gray squares denote the unit cell of the lattice. (b) Sections of the lattice potential along the dashed lines in (a).

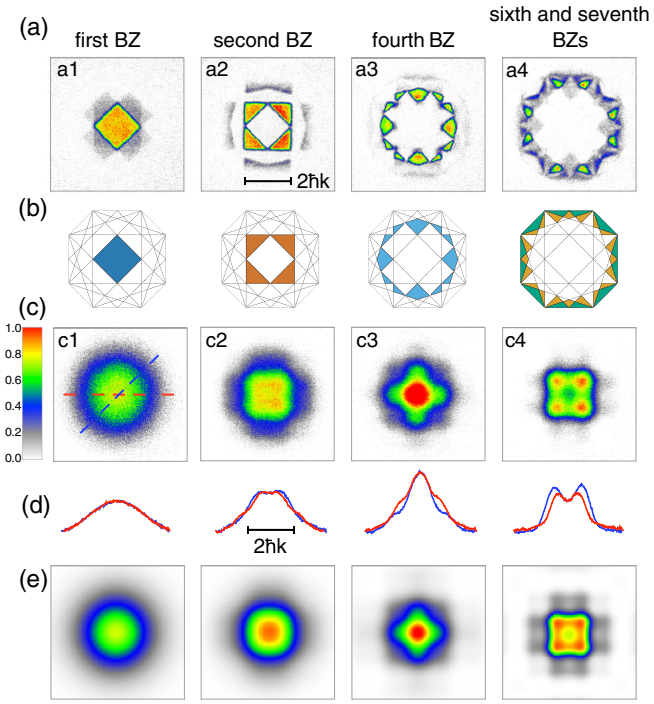

FIG. 2. (a) Band mapping images showing the population of the nth band in the nth Brillouin zones (BZs). Panel (a1) shows the case if no excitation is applied; the other panels [(a2)–(a4)] show the cases of excitation to the second, fourth, and seventh bands, respectively. (b) The map of BZs is shown with (from left to right) the first, second, fourth, and sixth and seventh BZs highlighted. (c) Regular momentum spectra corresponding to the band mapping images in (a). The color map on the left edge shows the normalized optical density. (d) Horizontal (red line graphs) and diagonal (blue line graphs) sections through the momentum spectra in (c) along the red dashed and blue dashed lines in (c1), respectively. (e) Momentum spectra for completely filled first, second, fourth, and seventh bands (from left to right) calculated for the same parameters as used in (c). The particle numbers in (c) and (e) are normalized to unity and parametrized with the same color map, shown in (c). In all plots in (a),(c)–(e) $V_0 = 12E_{\mathrm{rec}}$.

band [Figs 2(a2)–2(a4)]. These images were recorded after the atoms were held in the lattice for 50 ms with $V_0 = 12E_{\mathrm{rec}}$ and $\Delta V_f/V_0 \in \{-1.24, 0.314, 0.995, 1.703\}$. The choices of V_f adjusted for populating the second, fourth, and seventh bands, according to an exact band calculation, provide optimal selectivity since they maximize the gaps between the target band and adjacent bands (cf. Ref. [38]). A comparison with the theoretically expected Brillouin zones (BZs) in Fig. 2(b) shows that in Figs. 2(a2) and 2(a3) the second and fourth BZs are selectively populated, respectively, with remarkable efficiency. In Fig. 2(a4), the sixth and seventh BZ shows population in accordance with the expectation of a band crossing between the sixth and seventh band occurring during the band mapping procedure, as predicted by an exact band calculation (cf. Ref. [38]). The total fractions of atoms prepared in the first, second, fourth, and seventh bands, normalized to the total number of atoms initially loaded into the lattice, are 0.67, 0.67, 0.57, 0.62, respectively. Note that due to quantum pressure of the fermionic atoms, finite temperature, and the trap potential, without excitation, only $2/3$ of the atoms are prepared in the first band, while the rest is found in higher bands [cf. Fig. 2(a1)]. If we account for this circumstance and normalize the number of particles in the target bands after excitation by the number of atoms loaded to the first band, if no excitation is applied, one obtains remarkable fractions of 0.996, 0.84, and 0.92 for population of the second, fourth, and seventh bands, respectively. Very similar results are found for spin mixtures.

In Fig. 2(c), we show regular momentum spectra (cf. Ref. [38]), recorded after the atoms have dwelled for 50 ms in the lattice, which exhibit direct signatures of the orbital character of the optical lattices formed in the second, fourth, and seventh bands. The shown images directly correspond to the band mapping images in Fig. 2(a). These momentum spectra are expected to display squared absolute values of the Fourier transforms of the prevailing Wannier functions. For the case of Fig. 2(c1), the atoms reside in the local s orbitals of the lowest band, in accordance with the observation of a perfectly isotropic momentum distribution. In Fig. 2(c2), the second band is populated and, hence, the atoms populate both s orbitals in the shallow wells and p orbitals in the deep wells. In fact, the momentum distribution appears as a superposition of a large s-like component as in Fig. 2(c1), however less localized, and a small p-like component that displays a cloverleaf structure with an extra node in the center. This is better seen in the sections through the images Figs. 2(c1)–2(c4) shown in Fig. 2(d). The red (blue) line graphs show sections along the red dashed horizontal (blue dashed diagonal) line indicated in Fig. 2(c1). The superposition of s and p contributions explains the nearly flat top seen in the sections below Fig. 2(c2). In Fig. 2(e), calculated momentum spectra are shown, which reproduce the main features of the observations in Figs. 2(c1)–2(c4). The images in Fig. 2(e) result from an exact band calculation for the lattice parameters applied in Figs. 2(c1)–2(c4), neglecting the finite system size, the effect of the trap potential, and assuming that exclusively the target band is completely filled.

The lifetime for bosonic quantum gases in higher bands is limited by two-body s-wave collisions [24,26,27,42]. In Ref. [43], it has been shown that specific parameter configurations can be found, where different scattering processes destructively interfere with the result of remarkably long lifetimes on the order of several 100 ms. In the following, we explore the band decay dynamics after exciting a large fraction of fermionic atoms to the second band. In the case of spin-polarized samples, s-wave scattering is suppressed by Pauli's principle, and the first higher order scattering contribution, i.e., p-wave scattering, is negligible at the given low temperatures well below 100 nK. At the same time, collisions with hot background atoms are negligible on the few 10 s timescale, investigated here, as confirmed by the observation of lifetimes in the dipole trap of several minutes. Hence, interaction is expected to be practically irrelevant for band relaxation of spin-polarized samples. This gives rise to extreme band lifetimes, which are about 2 orders of magnitude longer than what has been observed with bosons. The main limitation is expected to arise through heating processes due to shaking of the lattice potential resonant with interband transitions. Heating with respect to the z direction, confined by a weak harmonic potential, is expected to be comparatively small. For a minimal model of the band decay dynamics, we consider the populations of the first and second bands, N_1 and N_2, respectively, and in addition the population N_L of all other bands, that are assumed not to be confined by the lattice potential and are hence considered as lost from the system. Heating couples the populations N_1 and N_2 by balanced transfer rates g_{12}. In addition, N_2 loses atoms toward N_L at a rate g_L, which gives rise to the two equations,

$$\begin{aligned} \dot{N}_1 &= g_{12}(N_2 - N_1), \\ \dot{N}_2 &= g_{12}(N_1 - N_2) - g_L N_2. \end{aligned} \tag{2}$$

This minimal rate equation model is illustrated in Fig. 3(a). At $t = 0$ about 10^5 spin-polarized fermions are prepared in the second band such that $N_2(0)/N_1(0) \approx 5$. The band mapping image in Fig. 3(a) shows the initial distribution of atoms across the BZs at $t = 10$ ms, confirming predominant occupation of the second BZ. The observed time evolution of $N_1(t)$ (red symbols) and $N_2(t)$ (blue symbols) is shown in Fig. 3(b). The model in Fig. 3(a) is used to determine the parameters $g_{12} = 0.0456 \pm 0.0015$ and $g_L = 0.0432 \pm 0.0009$ by simultaneously fitting with respect to both datasets in Fig. 3(b). An analytic solution of this model shows that the decay of $N_2(t)$ is exponential during the first 10 s with a $1/e$ decay time of 16.1 s.

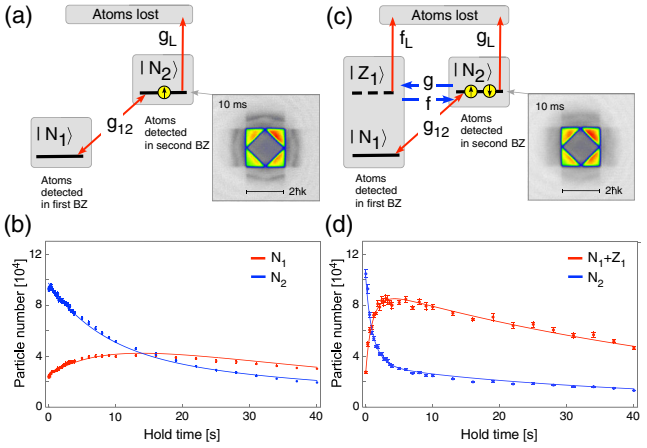

FIG. 3. (a) Model for band relaxation dynamics of spin-polarized samples after the second band is selectively populated, according to the band mapping image showing dominant population of the second BZ. (b) Observed populations in the first (N_1, red symbols) and second (N_2, blue symbols) bands are plotted versus the holding time. The solid traces result from the fit model in (a). (c) Extended relaxation model for balanced spin mixtures, including a class of atoms with population Z_1 residing in the first band with additional excitation of motion along the z axis. Binary collision processes (illustrated by blue arrows) exchange pairs of spin-up and spin-down particles between $|N_2\rangle$ and $|Z_1\rangle$. (d) Observed populations in the first ($N_1 + Z_1$, red symbols) and second (N_2, blue symbols) bands are plotted versus the holding time. The solid traces result from the fit model in (c). In (b) and (d), $V_0 = 7E_{\mathrm{rec}}$ and $\Delta V = 3.1E_{\mathrm{rec}}$. The error bars in (b) and (d) show statistical errors for averages of 20–30 experimental runs.

For mixtures of the two spin components $|m_F = -9/2\rangle$ and $|m_F = -7/2\rangle$, s-wave collisions between different spin states are possible. The singlet and triplet scattering lengths at zero magnetic field are $105a_0$ and $176a_0$, respectively ($a_0 =$ Bohr radius) [44]. For modeling band relaxation, only band-index changing collisions are relevant. We assume that, similarly as found for bosons in the same lattice potential [26,43], the dominant collisional process leading to loss of second band population is associated with a transfer of pairs of colliding spin-up and a spin-down atoms to the first band. Thereby, in fulfillment of energy-momentum conservation, an energy per particle of approximately the band gap between the first and second bands is deposited into motion along the z axis. Starting with a balanced spin mixture, it is reasonable to assume that the same dynamical evolution holds for both spin components. In the absence of binary collisions, we may hence describe each spin component by the same equations used for the spin-polarized case [Eq. (2)] with according particle numbers N_1 and N_2 representing the populations of either spin component in the first and second bands.

In an extended minimal relaxation model, including binary collision transfer between the second and first band, we have to consider an additional class of atoms with population Z_1 belonging to the first band but possessing additional excitation along the z axis with an energy similar to the band gap between the first and second band. Similarly as for the case of N_2, also Z_1 is subject to a decrease by heating toward the lost atom population N_L at a rate f_L. The decrease of N_2 toward Z_1 is modeled by a two-body collision term gN_2^2, with $g \equiv \beta/(2V_{N_2,\mathrm{eff}})$, where β denotes the two-body collision parameter and $V_{N_2,\mathrm{eff}}$ is the effective volume of the sample in the state $|N_2\rangle$ [45,46]. Conversely, the decrease of Z_1 toward N_2 is given by a two-body collision term fZ_1^2, with $f \equiv \beta/(2V_{Z_1,\mathrm{eff}})$, where $V_{Z_1,\mathrm{eff}}$ is the effective volume of the sample in the state $|Z_1\rangle$. We expect $V_{Z_1,\mathrm{eff}} > V_{N_1,\mathrm{eff}}$ and hence $f < g$. This relaxation model is sketched in Fig. 3(c) with the equations

$$\begin{aligned}\dot{N}_1 &= g_{12}(N_2 - N_1),\\ \dot{Z}_1 &= gN_2^2 - fZ_1^2 - f_L Z_1,\\ \dot{N}_2 &= fZ_1^2 - gN_2^2 + g_{12}(N_1 - N_2) - g_L N_2. \end{aligned} \tag{3}$$

In Fig. 3(d), initially most atoms are loaded into the second band, as illustrated by the band mapping image in Fig. 3(c), showing the initial distribution of atoms across the BZs at $t = 10$ ms with most atoms seen in the second BZ. The total populations detected in the first (red symbols) and second (blue symbols) bands, $N_1 + Z_1$ and N_2, respectively, are plotted versus the hold time. The solid lines are obtained by using the heating rates $g_{12} = 0.0456$ and $g_L = 0.0432$, found for the spin-polarized case, and by determination of $g = (6.472 \pm 0.234) \times 10^{-6}$, $f = (1.936 \pm 0.173) \times 10^{-6}$, and $f_L = 0.0167 \pm 0.0015$ via simultaneously fitting the model of Eq. (3) to both datasets in Fig. 3(d). Note that a significantly faster, clearly nonexponential decay of N_2 is observed as compared to Fig. 3(b). We may roughly estimate $\beta \approx \eta\sigma\bar{v}$, where $\sigma = 4\pi a^2$ is the free-space scattering cross section with the scattering length $a = 176a_0$, $\bar{v} = \sqrt{8k_BT/m\pi}$ is the mean thermal velocity for the temperature $T = 30$ nK, and m is the atomic mass of potassium. The factor η accounts for a transition matrix element involving the initial and final wave functions before and after the collision in the lattice potential. In previous experiments with bosons, small $\eta \ll 1$ have been found to give rise to long lifetimes of higher bands [24]. With $V_{N_2,\mathrm{eff}} \equiv N_2^2/\int dr^3 n_2^2(r) \approx 10^{-8}$ cm^3, where $n_2(r)$ is roughly approximated by the density profile in the dipole trap, one obtains $g \approx 6 \times 10^{-4}\eta$. By comparison with the value determined in the context of Eq. (3), one finds $\eta \approx 10^{-2}$.

In summary, selected excited Bloch bands of an optical square lattice have been loaded with a quantum degenerate Fermi gas with a single or two balanced spin components. In the former case, extreme band lifetimes (> 10 s) are observed as a result of the suppression of collisions due to Pauli's principle. For spin mixtures the lifetime is still on

the order of 1 s although limited by binary collisions between different spin components. The techniques demonstrated here form the basis for simulating fermionic superfluidity in orbital optical lattices. Similar techniques also apply for a wide range of other lattice geometries, including the hexagonal boron nitride lattice [47] or the Lieb lattice [48], known from cuprate high-temperature superconductors.

We acknowledge support from the Deutsche Forschungsgemeinschaft (DFG) through the collaborative research center SFB 925 (Project No. 170620586, C1). M. H. was partially supported by the Cluster of Excellence CUI: Advanced Imaging of Matter of the Deutsche Forschungsgemeinschaft (DFG)—EXC 2056—Project No. 390715994. We thank Lianghui Huang for useful discussions.

[1] G. Grynberg and C. Robilliard, Phys. Rep. **355**, 335 (2001).
[2] A. D. Ludlow, M. M. Boyd, J. Ye, E. Peik, and P. O. Schmidt, Rev. Mod. Phys. **87**, 637 (2015).
[3] R. P. Feynman, Int. J. Theor. Phys. **21**, 467 (1982).
[4] D. Jaksch, C. Bruder, J. I. Cirac, C. W. Gardiner, and P. Zoller, Phys. Rev. Lett. **81**, 3108 (1998).
[5] M. Lewenstein, A. Sanpera, V. Ahufinger, B. Damski, A. Sen(De), and U. Sen, Adv. Phys. **56**, 243 (2007).
[6] Ch. Gross and I. Bloch, Science **357**, 995 (2017).
[7] J. Hubbard, Proc. R. Soc. A. **276**, 238 (1963).
[8] R. Jördens, N. Strohmaier, K. Günter, H. Moritz, and T. Esslinger, Nature (London) **455**, 204 (2008).
[9] U. Schneider, L. Hackermüller, S. Will, Th. Best, I. Bloch, T. A. Costi, R. W. Helmes, D. Rasch, and A. Rosch, Science **322**, 1520 (2008).
[10] R. A. Hart *et al.*, Nature (London) **519**, 211 (2015).
[11] D. Greif, M. F. Parsons, A. Mazurenko, Ch. S. Chiu, S. Blatt, F. Huber, G. Ji, and M. Greiner, Science **351**, 953 (2016).
[12] P. T. Brown *et al.*, Science **357**, 1385 (2017).
[13] A. Mazurenko, C. S. Chiu, G. Ji, M. F. Parsons, M. Kanász-Nagy, R. Schmidt, F. Grusdt, E. Demler, D. Greif, and M. Greiner, Nature (London) **545**, 462 (2017).
[14] L. Tarruell and L. Sanchez-Palencia, C. R. Phys. **19**, 365 (2018).
[15] Y. Tokura and N. Nagaosa, Science **288**, 462 (2000).
[16] S. Maekawa, T. Tohyama, S. E. Barnes, S. Ishihara, W. Koshibae, and G. Khaliullin, *Springer Series in Solid-State Sciences* (Springer, New York, 2004), Vol. 144.
[17] M. R. Slot, S. N. Kempkes, E. J. Knol, W. M. J. van Weerdenburg, J. J. van den Broeke, D. Wegner, D. Vanmaekelbergh, A. A. Khajetoorians, C. Morais Smith, and I. Swart, Phys. Rev. X **9**, 011009 (2019).
[18] I. Bloch, J. Dalibard, and W. Zwerger, Rev. Mod. Phys. **80**, 885 (2008).
[19] J. Weiner, *Cold and Ultracold Collisions in Quantum Microscopic and Mesoscopic Systems* (Cambridge University Press, Cambridge, England, 2003).
[20] C. Chin, R. Grimm, P. Julienne, and E. Tiesinga, Rev. Mod. Phys. **82**, 1225 (2010).
[21] G. Wirth, M. Ölschläger, and A. Hemmerich, Nat. Phys. **7**, 147 (2011).
[22] M. Ölschläger, G. Wirth, and A. Hemmerich, Phys. Rev. Lett. **106**, 015302 (2011).
[23] M. Lewenstein and W. V. Liu, Nat. Phys. **7**, 101 (2011).
[24] T. Kock, C. Hippler, A. Ewerbeck, and A. Hemmerich, J. Phys. B **49**, 042001 (2016).
[25] V. M. Stojanović, C. Wu, W. V. Liu, and S. Das Sarma, Phys. Rev. Lett. **101**, 125301 (2008).
[26] S. Paul and E. Tiesinga, Phys. Rev. A **88**, 033615 (2013).
[27] X. Li and W. V. Liu, Rep. Prog. Phys. **79**, 116401 (2016).
[28] M. Greiner, C. A. Regal, and D. S. Jin, Nature (London) **426**, 537 (2003).
[29] S. Jochim, M. Bartenstein, A. Altmeyer, G. Hendl, S. Riedl, C. Chin, J. H. Denschlag, and R. Grimm, Science **302**, 2101 (2003).
[30] M. W. Zwierlein, C. A. Stan, C. H. Schunck, S. M. F. Raupach, S. Gupta, Z. Hadzibabic, and W. Ketterle, Phys. Rev. Lett. **91**, 250401 (2003).
[31] C. A. Regal, M. Greiner, and D. S. Jin, Phys. Rev. Lett. **92**, 040403 (2004).
[32] M. Bartenstein, A. Altmeyer, S. Riedl, S. Jochim, C. Chin, J. H. Denschlag, and R. Grimm, Phys. Rev. Lett. **92**, 120401 (2004).
[33] M. W. Zwierlein, C. A. Stan, C. H. Schunck, S. M. F. Raupach, A. J. Kerman, and W. Ketterle, Phys. Rev. Lett. **92**, 120403 (2004).
[34] T. Bourdel, L. Khaykovich, J. Cubizolles, J. Zhang, F. Chevy, M. Teichmann, L. Tarruell, S. J. J. M. F. Kokkelmans, and C. Salomon, Phys. Rev. Lett. **93**, 050401 (2004).
[35] G. B. Partridge, K. E. Strecker, R. I. Kamar, M. W. Jack, and R. G. Hulet, Phys. Rev. Lett. **95**, 020404 (2005).
[36] M. W. Zwierlein, J. R. Abo-Shaeer, A. Schirotzek, C. H. Schunck, and W. Ketterle, Nature (London) **435**, 1047 (2005).
[37] M. Randeria, W. Zwerger, and M. Zwierlein, *Lecture Notes in Physics* (Springer, Berlin, 2012), Vol. 836.
[38] See Supplemental Material at http://link.aps.org/supplemental/10.1103/PhysRevLett.127.033201 for details on the experimental setup and protocols, which includes Refs. [39–41].
[39] A. Hemmerich, D. Schropp, Jr., and T. W. Hänsch, Phys. Rev. A **44**, 1910 (1991).
[40] D. Rio Fernandes, F. Sievers, N. Kretzschmar, S. Wu, C. Salomon, and F. Chevy, Europhys. Lett. **100**, 63001 (2012).
[41] S. Rosi, A. Burchianti, S. Conclave, D. S. Naik, G. Roati, C. Fort, and F. Minardi, Sci. Rep. **8**, 1301 (2018).
[42] W. V. Liu and C. Wu, Phys. Rev. A **74**, 013607 (2006).
[43] M. Nuske, J. Vargas, M. Hachmann, R. Eichberger, L. Mathey, and A. Hemmerich, Phys. Rev. Research **2**, 043210 (2020).
[44] J. L. Bohn, Phys. Rev. A **61**, 053409 (2000).
[45] J. Weiner, V. S. Bagnato, S. Zilio, and P. S. Julienne, Rev. Mod. Phys. **71**, 1 (1999).
[46] D. Hansen and A. Hemmerich, Phys. Rev. Lett. **96**, 073003 (2006).
[47] M. Weinberg, C. Staarmann, C. Ölschläger, J. Simonet, and K. Sengstock, 2D Mater. **3**, 024005 (2016).
[48] M. Di Liberto, A. Hemmerich, and C. Morais Smith, Phys. Rev. Lett. **117**, 163001 (2016).